

On Embedding B-Splines in Recursive State Estimation

Kailai Li

Abstract

We present a principled study on establishing a novel probabilistic framework for state estimation. B-splines are embedded in the state-space modeling as a continuous-time intermediate between the states of recurrent control points and asynchronous sensor measurements. Based thereon, the spline-embedded recursive estimation scheme is established w.r.t. common sensor fusion tasks, and the corresponding technique for modeling uncertain motion estimates is introduced. We evaluate the proposed estimation scheme using real-world-based synthesized data with a range-inertial setting. The numerical results demonstrate several advantages of spline embedding in recursive state estimation over the classic discrete-time filtering scheme.

Index Terms

Estimation, filtering, stochastic systems, robotics

I. INTRODUCTION

State estimation plays a critical role in ubiquitous application scenarios related to systems and control, including tasks such as object tracking, motion planning, robotic manipulation and locomotion, as well as cyber-physical security [1]–[4]. In most engineering practices, performing state estimation typically involves incorporating asynchronous measurements of various sensing modalities, such as wheel odometry, camera, ultra-wideband (UWB), light detection and ranging (LiDAR), and inertial measurement unit (IMU) [5]–[8].

The classic methods for multi-sensor fusion are rooted in the recursive Bayesian estimation scheme. In the context of estimating motions, popular choices of approaches include the extended Kalman filter (EKF) [9] and the particle filter [10]. The state-space representation is herein exploited to describe uncertain physical systems with a composition of the process and measurement models under uncertainty. State estimates are delivered recursively based thereon via prediction and update steps over time [11]. This probabilistic scheme also directly provides uncertainty quantification of the estimate, allowing for further tasks, such as outlier rejection, planning, decision and control, to be conducted with adequate accuracy and confidence [12]–[15]. To estimate the six-DoF rigid-body motions, recursive estimation approaches have also been developed w.r.t. nonlinear manifolds using error-state formulation and geometry-driven methodologies [16]–[18].

The conventional recursive estimation scheme is based on the Markov assumption, which requires sufficient knowledge of the underlying system dynamics and disregards state propagation beyond consecutive time steps. Recent advances in robotics, particularly in simultaneous localization and mapping, have introduced alternative schemes using optimization [19]. Optimal state estimates are obtained in the sense of nonlinear least squares (NLS), with residual terms built upon multi-sensor measurements through a graph structure over a certain time span. Compared with the recursive scheme, this paradigm shift can lead to improved estimation accuracy while maintaining tractable computational cost due to the sparse problem

This work is supported by the Swedish Research Council under grant Scalable Kalman Filters. (*Corresponding author: Kailai Li.*) Kailai Li is with the Division of Automatic Control, Department of Electrical Engineering, Linköping University, 58183 Linköping, Sweden (e-mail: kailai.li@liu.se).

structure [20]. Based thereon, numerous state-of-the-art solutions have emerged in robotic state estimation and perception using multi-sensor setups. A variety of important techniques, including IMU preintegration and keyframe-based sliding-window optimization, have been proposed to achieve high-performance state estimation in terms of tracking accuracy, robustness and runtime efficiency [21]–[25].

In state estimation, the random variables are driven by the underlying stochastic dynamics that is inherently continuous over time, whereas observed at discrete time instants with noise. To properly address this discrepancy, most recursive estimation schemes rely on temporal discretizations of the continuous-time state-space models, resulting in the continuous-discrete and discrete-time variants [26]. For that, remedies such as oversampling of the system or approximation of transition densities have been introduced, and additional efforts are typically required for achieving viable accuracy and stability [27]. Given asynchronous sensor readings, delivering state estimates at the desired time instants (e.g., at a fixed frame rate) inevitably requires certain approximation, such as linear interpolation [6], [23]. Besides, sensor measurements that contribute to the state propagation are often assumed to be constant over the sampling interval. These operations can introduce additional errors and often require tedious implementation, especially when combined with other procedures, e.g., the IMU preintegration [23]. Furthermore, enforcing kinematic relations over sequential motion estimates in conjunction with sensor fusion is hardly possible without introducing explicit constraints. Under unfavorable conditions, such as highly dynamic motions and noisy measurements with outliers, state estimates can exhibit physically infeasible transitions.

There have been increasing efforts to enable continuous-time sensor fusion, and significant progress has been made in utilizing the B-spline [28], [29]. Established atop a series of control points (knots), B-splines parameterize motion trajectories as polynomial functions over time, leading to a more efficient state representation in comparison with the discrete-time counterpart [30]. B-splines are smooth to a given order and inherently guarantee kinematic relations over temporal differentiations. Additionally, the locality of B-splines enables convenient interpolations via matrix multiplication and implicitly spreads correlations over dynamical motions through adjacent control points [31]. Using the cumulative form of B-splines, it is also possible to extend their utility from modeling vector-valued (Euclidean) to Lie group-valued functions. This makes them particularly appealing for continuous-time parameterization of six-DoF pose trajectories in various robotic applications [7], [32], [33].

Based on the methodology of B-spline fitting, a few systems have been recently developed for continuous-time state estimation using multi-sensor setups. These involve, in particular, the combination of the IMU with (event) camera, radar, UWB, and LiDAR, among other modalities [7], [30], [34]–[38]. In these systems, the control points of B-splines are obtained optimally via NLS, with residuals directly comparing the sensor measurement and the corresponding interpolated value. To realize high-performance sensor fusion, several important theories and approaches have been introduced, including quaternion-based B-spline modeling, efficient temporal and spatial differentiations, as well as sliding-window spline fitting [7], [39], [40].

Though ongoing progress has been made in utilizing B-splines for sensor fusion, all existing methods are optimization-based, leaving a considerable gap towards establishing a self-contained probabilistic framework. Besides, relevant works only refer to applying recursive filters to spline approximation for geometry modeling [41], [42]. To the best knowledge of the author, there is currently no published work that systematically exploits B-splines in recursive state estimation of dynamical systems.

Contributions

In light of the current state of the art, we propose a novel recursive state estimation scheme for continuous-time sensor fusion. Cubic B-splines are exploited for state parameterization with kinematic interpolations unified as a concise matrix representation (Sec. III). Further, we introduce the so-called spline-state-space (TriS) model based on the concept of recurrent control points, endowing recursive feasibility and inferential power to cubic B-splines in state estimation (Sec. IV). This also leads to expressive dynamical modeling, meanwhile utilizing the appealing locality and smoothness of B-splines.

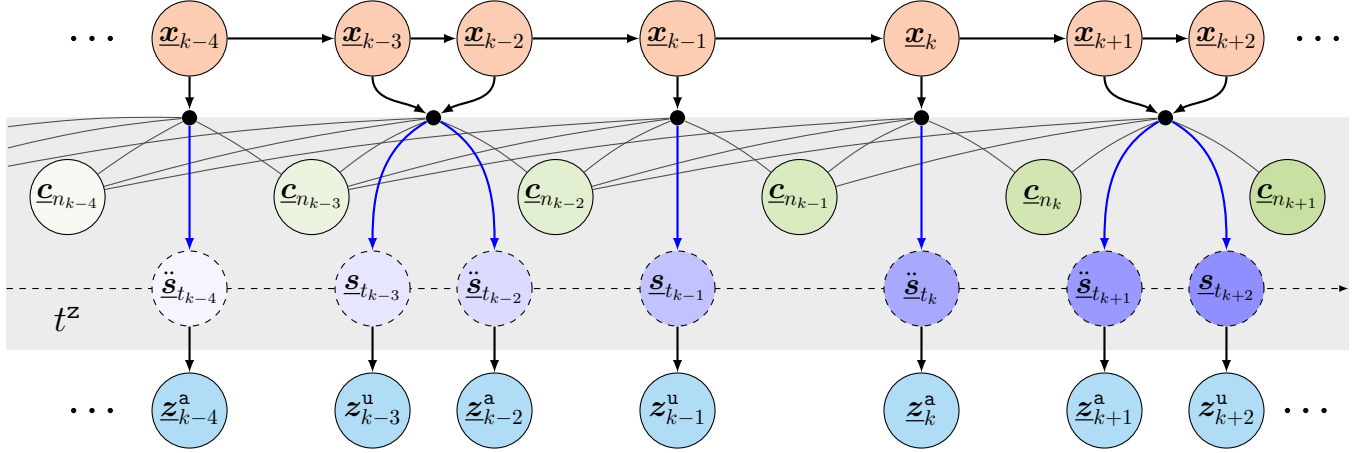


Fig. 1: Graph representation of the proposed spline-state-space (TriS) model. A cubic B-spline is embedded to state-space modeling as a continuous-time intermediate (area in gray) bridging the discrete-time state transition and observation. Nodes of recurrent control points (lime green) in the states (red) and interpolated dynamical motions (purple) queried by the measurements (blue) are rendered w.r.t. time. We hereby showcase asynchronous ultra-wideband and accelerometer measurements (denoted by superscripts u and a , respectively) given by the position and acceleration interpolations, \underline{z} and $\underline{\ddot{z}}$, respectively.

Afterward, the spline-embedded recursive estimation (SERE) scheme is newly established with corresponding probabilistic modeling of motion estimates (Sec. V). We further evaluate the SERE scheme on a real-world-based synthetic data set using a range-inertial setting (Sec. VI). The numerical results show that the spline embedding enables considerable improvements on tracking performance compared to the conventional filtering scheme. As the first fundamental study on spline-based recursive state estimation, our work sketches out a self-contained paradigm for continuous-time probabilistic sensor fusion.

II. NOTATION CONVENTIONS

Throughout the following content, we use underlined lowercase variables, such as $\underline{x} \in \mathbb{R}^d$, to denote vectors, with letter d denoting the dimension of Euclidean spaces. Random variables are indicated by lowercase letters of bold font, such as $\underline{\mathbf{x}} \in \mathbb{R}^d$. Matrices are written as uppercase letters of bold case, such as $\mathbf{D} \in \mathbb{R}^{d \times d}$. We use $\mathbf{I}_d \in \mathbb{R}^{d \times d}$ and $\mathbf{0}_d \in \mathbb{R}^{d \times d}$ to denote d -dimensional identity and zero matrices, respectively. In the context of recursive state estimation, we exploit $k \in \mathbb{N}$ to denote a discrete time step, whereas the exact time instant at k is written as lowercase letter t_k . Moreover, we exploit calligraphic lowercase letters to denote functions, such as $\underline{a}(x)$ and $\underline{a}(x)$ for scalar- and vector-valued functions, respectively. The operator \otimes denotes the Kronecker product, and the operator \oplus stands for the direct sum of two matrices [43].

III. CONTINUOUS-TIME MOTION REPRESENTATION

For demonstrating our work in this paper, we express B-splines using their cubic form (fourth-order) in d -dimensional Euclidean spaces. Note that the presented techniques can be extended to B-splines of higher orders in a straightforward manner. Cubic B-splines exhibit continuous-time derivatives up to the second order, which is sufficient for fusing measurements of most sensory modalities related to motion estimation, including the accelerometer [7], [37], [38].

Given a set of control points $\{c_i\}_{i=1}^n \subset \mathbb{R}^d$ at time instants $\{t_i\}_{i=1}^n \subset \mathbb{R}$ of uniform temporal interval τ , a cubic B-spline can be established for trajectory representation. At an arbitrary time instant $t \in (t_i, t_{i+1}]$, the trajectory point is determined by a local set of control points $\{c_{i+j-2}\}_{j=0}^3$ according to

$$\underline{z}_t = \mathbf{C}_i \boldsymbol{\Omega} \underline{u}_t, \quad (1)$$

with matrix

$$\mathbf{C}_i = [\underline{c}_{i-2}, \underline{c}_{i-1}, \underline{c}_i, \underline{c}_{i+1}] \in \mathbb{R}^{d \times 4}$$

concatenating the corresponding control points columnwise. The vector \underline{u}_t is given by

$$\underline{u}_t = [1, u_t, u_t^2, u_t^3]^\top \in \mathbb{R}^4,$$

which contains the powers of the normalized time instant

$$u_t = (t - t_i)/\tau. \quad (2)$$

Ω is the *basis function matrix* of cubic B-splines and follows

$$\Omega = \frac{1}{6} \begin{bmatrix} 1 & -3 & 3 & -1 \\ 4 & 0 & -6 & 3 \\ 1 & 3 & 3 & -3 \\ 0 & 0 & 0 & 1 \end{bmatrix}. \quad (3)$$

We can derive the velocity trajectory of cubic B-splines by taking the first derivative of the polynomial function (1) w.r.t. time. It is given by

$$\dot{\underline{z}}_t = \mathbf{C}_i \Omega \dot{\underline{u}}_t, \quad \text{with} \quad \dot{\underline{u}}_t = [0, 1, 2u_t, 3u_t^2]^\top / \tau. \quad (4)$$

Further, the acceleration trajectory can be derived as the following function over time

$$\ddot{\underline{z}}_t = \mathbf{C}_i \Omega \ddot{\underline{u}}_t, \quad \text{with} \quad \ddot{\underline{u}}_t = [0, 0, 2, 6u_t]^\top / \tau^2. \quad (5)$$

In the following content, we use \circ atop the spline function \underline{z}_t , i.e., $\overset{\circ}{\underline{z}}_t$, to denote trajectories of different orders at time instant t (including \underline{z}_t , $\dot{\underline{z}}_t$, and $\ddot{\underline{z}}_t$). Therefore, the kinematic interpolations can be unified as

$$\overset{\circ}{\underline{z}}_t = \mathbf{C}_i \Omega \overset{\circ}{\underline{u}}_t, \quad (6)$$

with $\overset{\circ}{\underline{u}}_t$ concretized in (1), (4), and (5).

IV. STOCHASTIC MODELING ON B-SPLINES

In existing spline-based sensor fusion schemes, control points over a certain time span are optimally obtained in the sense of nonlinear least squares, delivering motion trajectories as continuous functions over time. The kinematic interpolations in Sec. III provide computational foundations for computing residuals using measurements at original time instants [7], [39]. However, modeling the uncertainty of motion estimates is almost infeasible within an optimization-based scheme. Thus, we aim to establish a principled framework for stochastic modeling using B-splines.

A. Vectorized Kinematic Interpolations

We now express the basic kinematic interpolations introduced in Sec. III using a vector representation of the control points. According to [44], we can perform vectorization on both sides of (6) and obtain

$$\begin{aligned} \text{vec}(\overset{\circ}{\underline{z}}_t) &= \text{vec}(\mathbf{C}_i \Omega \overset{\circ}{\underline{u}}_t) \\ &= ((\Omega \overset{\circ}{\underline{u}}_t)^\top \otimes \mathbf{I}_d) \text{vec}(\mathbf{C}_i), \end{aligned}$$

with $t \in (t_i, t_{i+1}]$. \otimes denotes the Kronecker product as introduced in Sec. II. Note that $\overset{\circ}{\underline{z}}_t$ is a d -dimensional vector. It then follows

$$\overset{\circ}{\underline{z}}_t = \overset{\circ}{\Lambda}_t \underline{x}_i, \quad \text{with} \quad \overset{\circ}{\Lambda}_t = (\Omega \overset{\circ}{\underline{u}}_t)^\top \otimes \mathbf{I}_d \in \mathbb{R}^{d \times 4d} \quad (7)$$

containing the interpolation coefficients w.r.t. control points that are combined in the vector

$$\underline{x}_i = \text{vec}(\mathbf{C}_i) = [\underline{c}_{i-2}^\top, \underline{c}_{i-1}^\top, \underline{c}_i^\top, \underline{c}_{i+1}^\top]^\top \in \mathbb{R}^{4d}.$$

B. Spline-State-Space (TriS) Model

In the context of recursive Bayesian estimation, B-splines can be leveraged for continuous-time parameterization of dynamical motions w.r.t. discrete-time observations. We conceptualize this idea into the so-called spline-state-space (TriS) model as illustrated by the graph representation in Fig. 1. A B-spline is embedded to a typical state-space model as an intermediate between the discrete-time states and observations.

1) *State vector*: Given the measurements $\{\underline{z}_i\}_{i=1}^k$, the cubic B-spline is maintained using a minimal set of control points $\{\underline{c}_i\}_{i=1}^{n_k}$ at time instants $\{t_i\}_{i=1}^{n_k}$, with the latest measurement time instant $t_k^z \in (t_{n_k-1}, t_{n_k}]$. The kinematic interpolation at time step k is then determined by the latest four control points $\{\underline{c}_{n_k-i}\}_{i=0}^3$, which we compose into the following state vector

$$\underline{\mathbf{x}}_k = [\underline{\mathbf{c}}_{n_k-3}^\top, \underline{\mathbf{c}}_{n_k-2}^\top, \underline{\mathbf{c}}_{n_k-1}^\top, \underline{\mathbf{c}}_{n_k}^\top]^\top \in \mathbb{R}^{4d}. \quad (8)$$

We name this local set of control points as the *recurrent control points* to highlight their temporal relations to the most recent measurement \underline{z}_k .

2) *Measurement model*: Given the state vector in (8), the measurement model at time step k can be expressed as the following general form

$$\underline{z}_k = \underline{h}_{t_k^z}(\underline{\mathbf{x}}_k) + \underline{\mathbf{v}}_k, \quad \text{with } t_k^z \in (t_{n_k-1}, t_{n_k}]. \quad (9)$$

We use \mathbb{Z} to denote the domain of measurements. $\underline{\mathbf{v}}_k \in \mathbb{Z}$ is an additive noise assumed to be zero-mean Gaussian-distributed, i.e., $\underline{\mathbf{v}}_k \sim \mathcal{N}(\underline{\mathbf{0}}, \mathbf{R}_k)$, with \mathbf{R}_k being the measurement noise covariance. The observation function $\underline{h}_{t_k^z} : \mathbb{R}^{4d} \rightarrow \mathbb{Z}$ takes the recurrent control points at time step k as input and can be decomposed into two cascaded steps as follows

$$\underline{h}_{t_k^z}(\underline{\mathbf{x}}_k) = \underline{\ell}(\underline{j}_{t_k^z}(\underline{\mathbf{x}}_k)). \quad (10)$$

The function $\underline{j}_{t_k^z} : \mathbb{R}^{4d} \rightarrow \mathbb{R}^d$ denotes the vectorized kinematic interpolation introduced in (7) at time instant t_k^z , generating the motion variable for sensing. Further, function $\underline{\ell} : \mathbb{R}^d \rightarrow \mathbb{Z}$ models the actual sensory modality, mapping the interpolated motion to the noise-free observation. In Fig. 1, this cascaded measurement modeling is showcased with an ultra-wideband-accelerometer setup.

3) *Process model*: The process model describes the propagation of recurrent control points in the case that the incoming measurement falls outside the current spline time span. Suppose that the measurement \underline{z}_{k+1} comes at time instant $t_{k+1}^z \in (t_{n_k}, t_{n_k} + \tau]$, given the spline of n_k control points. In order to accommodate the measurement model at t_{k+1}^z as introduced in (9), the spline is extended to $n_{k+1} = n_k + 1$ control points. Consequently, the state vector defined in (8) is updated to

$$\begin{aligned} \underline{\mathbf{x}}_{k+1} &= [\underline{\mathbf{c}}_{n_{k+1}-3}^\top, \underline{\mathbf{c}}_{n_{k+1}-2}^\top, \underline{\mathbf{c}}_{n_{k+1}-1}^\top, \underline{\mathbf{c}}_{n_{k+1}}^\top]^\top \\ &= [\underline{\mathbf{c}}_{n_k-2}^\top, \underline{\mathbf{c}}_{n_k-1}^\top, \underline{\mathbf{c}}_{n_k}^\top, \underline{\mathbf{c}}_{n_k+1}^\top]^\top, \end{aligned} \quad (11)$$

where the first three control points overlap with the last three control points in the previous state $\underline{\mathbf{x}}_k$ in (8). In general, the process model can be expressed as

$$\underline{\mathbf{x}}_{k+1} = \underline{\mathcal{a}}(\underline{\mathbf{x}}_k) + \underline{\mathbf{w}}_{k+1}. \quad (12)$$

The additive process noise $\underline{\mathbf{w}}_{k+1} \in \mathbb{R}^{4d}$ is assumed to follow a zero-mean Gaussian distribution $\mathcal{N}(\underline{\mathbf{0}}, \mathbf{Q}_{k+1})$, with \mathbf{Q}_{k+1} being the covariance. The transition function $\underline{\mathcal{a}} : \mathbb{R}^{4d} \rightarrow \mathbb{R}^{4d}$ in (12) can be established with reference to various dynamical principles. We hereby introduce a straightforward strategy with the following two steps: 1) we retain the first three control points $\{\underline{\mathbf{c}}_{n_k-i}\}_{i=0}^2$ in $\underline{\mathbf{x}}_{k+1}$ at their coordinates in the previous state $\underline{\mathbf{x}}_k$, and 2) the latest control point $\underline{\mathbf{c}}_{n_k+1}$ is added by preserving the velocity at the

Algorithm 1: Spline-Embedded Recursive Estimation

Input: posterior estimate $\hat{\underline{x}}_{k-1|k-1}$, $\mathbf{P}_{k-1|k-1}$ measurement \underline{z}_k at t_k^z , number of knots n_{k-1}

Output: posterior estimate $\hat{\underline{x}}_{k|k}$, $\mathbf{P}_{k|k}$

```

1 if  $t_k^z > t_{n_{k-1}}$  then
  /* prediction */
2    $n_k \leftarrow n_{k-1} + 1$ ;
3    $\hat{\underline{x}}_{k|k-1} \leftarrow \mathbf{A}\hat{\underline{x}}_{k-1|k-1}$ ;
4    $\mathbf{P}_{k|k-1} \leftarrow \mathbf{A}\mathbf{P}_{k-1|k-1}\mathbf{A}^\top + \mathbf{Q}_k$ ;
5 else
6    $n_k \leftarrow n_{k-1}$ ;
7    $\hat{\underline{x}}_{k|k-1} \leftarrow \hat{\underline{x}}_{k-1|k-1}$ ;
8    $\mathbf{P}_{k|k-1} \leftarrow \mathbf{P}_{k-1|k-1}$ ;
  /* update */
9  $\mathbf{H}_k \leftarrow \mathcal{F}_{\hat{\underline{x}}_{k|k-1}}(\hat{\underline{x}}_{k|k-1})\hat{\mathbf{A}}_{t_k^z}$ ; // see (14)
10  $\mathbf{K}_k \leftarrow \mathbf{P}_{k|k-1}\mathbf{H}_k^\top(\mathbf{H}_k\mathbf{P}_{k|k-1}\mathbf{H}_k^\top + \mathbf{R}_k)^{-1}$ ;
11  $\hat{\underline{x}}_{k|k} \leftarrow \hat{\underline{x}}_{k|k-1} + \mathbf{K}_k(\underline{z}_k - \underline{\mathcal{H}}_{t_k^z}(\hat{\underline{x}}_{k|k-1}))$ ;
12  $\mathbf{P}_{k|k} \leftarrow (\mathbf{I} - \mathbf{K}_k\mathbf{H}_k)\mathbf{P}_{k|k-1}$ ;
13 return  $\hat{\underline{x}}_{k|k}$ ,  $\mathbf{P}_{k|k}$ 

```

time instant $t_{n_{k-1}}$. For the latter step, we perform velocity interpolations at time instants $t_{n_{k-1}}$ and t_{n_k+1} according to (4), resulting in

$$\begin{aligned} \dot{\underline{c}}_{t_{n_{k-1}}} &= \frac{\underline{c}_{n_k-1} - \underline{c}_{n_k-3}}{2\tau} \quad \text{and} \\ \dot{\underline{c}}_{t_{n_k+1}} &= \frac{\underline{c}_{n_k+1} - \underline{c}_{n_k-1}}{2\tau}, \end{aligned}$$

respectively. Imposing identical velocities at these two time instants then yields

$$\underline{c}_{n_k+1} = 2\underline{c}_{n_k-1} - \underline{c}_{n_k-3}.$$

Therefore, the process model in (12) can be concretized as the following linear expression

$$\underline{\mathbf{x}}_{k+1} = \mathbf{A}\underline{\mathbf{x}}_k + \underline{\mathbf{w}}_{k+1}, \quad (13)$$

with the transition matrix given by

$$\mathbf{A} = \begin{bmatrix} \mathbf{0}_d & \mathbf{I}_d & \mathbf{0}_d & \mathbf{0}_d \\ \mathbf{0}_d & \mathbf{0}_d & \mathbf{I}_d & \mathbf{0}_d \\ \mathbf{0}_d & \mathbf{0}_d & \mathbf{0}_d & \mathbf{I}_d \\ -\mathbf{I}_d & \mathbf{0}_d & 2\mathbf{I}_d & \mathbf{0}_d \end{bmatrix}.$$

V. SPLINE EMBEDDING IN RECURSIVE ESTIMATION

Based on the proposed spline-state-space model, the task of continuous-time motion estimation can be converted into estimating discrete-time recurrent control points. To concretize this concept, we now introduce the so-called spline-embedded recursive estimation (SERE) scheme together with a simple case study in this section.

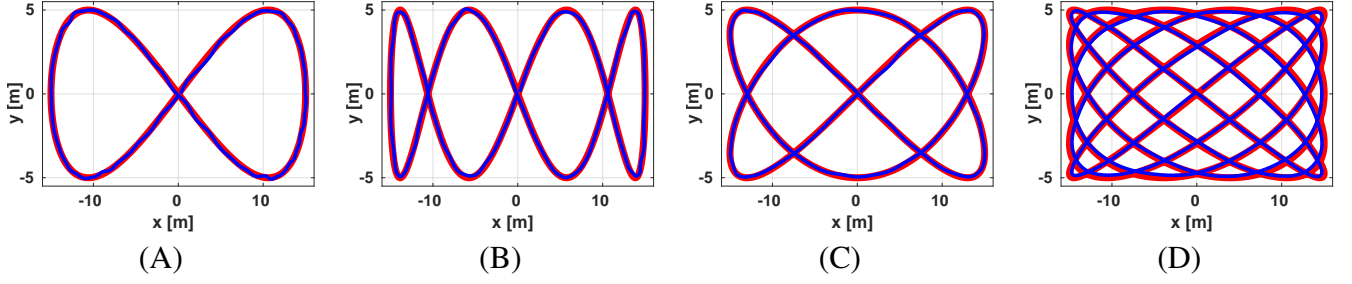


Fig. 2: Exemplary runs of spline-embedded recursive estimation for positioning along various Lissajous curves as discussed in Sec. V-C. Blue and red trajectories indicate the estimates and the ground truth, respectively.

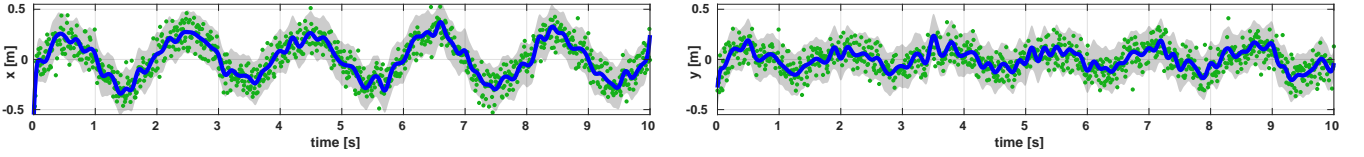


Fig. 3: Estimates on the x and y axes over the sequence drawn in Fig. 2-(D). The means are depicted w.r.t. the ground truth in blue, and the uncertainty is plotted in gray using one standard deviation. Green dots indicate the position measurements.

A. Spline-Embedded Recursive Estimation (SERE)

As shown in Alg. 1, the recurrent control points are estimated recursively following the concept of Kalman filtering based on the TriS model. Suppose that a measurement \underline{z}_k is obtained at time instant t_k^z , given n_{k-1} control points. The state \underline{x}_{k-1} composes recurrent control points $\{\underline{c}_{n_{k-1}-i}\}_{i=0}^3$, and its previous posterior estimate mean $\hat{\underline{x}}_{k-1|k-1}$ and covariance $\mathbf{P}_{k-1|k-1}$ are available. If the measurement time instant exceeds the current spline time span, namely, $t_k^z > t_{n_{k-1}}$, we perform state propagation according to the system model in (13), leading to $n_k = n_{k-1} + 1$ control points and the predicted prior estimate (Alg. 1, lines 1–4). Otherwise, the previous state estimate remains as the prior, with the number of control points being unchanged (Alg. 1, lines 5–8). During the update step, a basic strategy is to linearize the observation function (10) in the measurement model (9) at the prior estimate mean $\hat{\underline{x}}_{k|k-1}$. The resulting observation matrix can be obtained by applying the chain rule as

$$\begin{aligned} \mathbf{H}_k &= \mathcal{F}_{\underline{\ell}}(\underline{\dot{\mathbf{j}}}_{t_k^z}(\hat{\underline{x}}_{k|k-1})) \mathcal{F}_{\underline{\dot{\mathbf{j}}}_{t_k^z}}(\hat{\underline{x}}_{k|k-1}) \\ &= \mathcal{F}_{\underline{\ell}}(\underline{\dot{\mathbf{j}}}_{t_k^z}(\hat{\underline{x}}_{k|k-1})) \mathbf{\Lambda}_{t_k^z}, \end{aligned} \quad (14)$$

with the first term being the Jacobian of the sensing function $\underline{\ell}$ w.r.t. the kinematic motion $\underline{\dot{\mathbf{j}}}$ interpolated at t_k^z using the prior estimate $\hat{\underline{x}}_{k|k-1}$. The second term in (14) refers to the Jacobian of the kinematic interpolation function $\underline{\dot{\mathbf{j}}}$ w.r.t. the state vector. According to the linear expression given in (7), it follows

$$\mathcal{F}_{\underline{\dot{\mathbf{j}}}_{t_k^z}}(\hat{\underline{x}}_{k|k-1}) = \mathbf{\Lambda}_{t_k^z},$$

which is constant given the measurement time instant t_k^z and the order of kinematic motion observed by the sensor (Alg. 1, line 9). Based thereon, the prior estimate can be corrected by incorporating the measurement \underline{z}_k through a typical EKF update step, yielding the posterior estimate mean $\hat{\underline{x}}_{k|k}$ and covariance $\mathbf{P}_{k|k}$ (Alg. 1, line 10–13).

B. Probabilistic Interpolation

Embedding B-splines in recursive estimation decouples discrete-time state propagation from sensing continuous-time dynamical motions. Given the state estimate of mean $\hat{\underline{x}}_k$ and covariance \mathbf{P}_k , we now aim to retrieve the motion estimates $\{\hat{\underline{s}}_{t_i}\}_{i=1}^m$ at arbitrary time instants $\{t_i\}_{i=1}^m \subset (t_{n_{k-1}}, t_{n_k}]$. For that, the queried motions are stacked into a vector

$$\hat{\underline{s}}_{t_{1:m}} = [\hat{\underline{s}}_{t_1}^\top, \dots, \hat{\underline{s}}_{t_m}^\top]^\top \in \mathbb{R}^{dm}, \quad (15)$$

to which we perform (7) in a batchwise manner. The kinematic interpolations are linear w.r.t. recurrent control points. Thus, the mean and covariance of the motion estimates in (15) follow

$$\hat{\underline{\mu}}_{t_{1:m}} = \hat{\Lambda}_{t_{1:m}} \hat{\underline{x}}_k \quad \text{and} \quad \hat{\Sigma}_{t_{1:m}} = \hat{\Lambda}_{t_{1:m}} \mathbf{P}_k \hat{\Lambda}_{t_{1:m}}^\top, \quad (16)$$

respectively, where the matrix

$$\hat{\Lambda}_{t_{1:m}} = [\hat{\Lambda}_{t_1}^\top, \dots, \hat{\Lambda}_{t_m}^\top]^\top \in \mathbb{R}^{dm \times 4d}$$

denotes the combined coefficient matrices at each time instant. Thus, we essentially obtain the joint probability distribution of the dynamical motion estimates at any time instants, with different orders of temporal derivatives unified within a single computational procedure. To showcase the utility of the proposed SERE scheme, we now present a brief case study as follows.

C. Case Study

We synthesize a localization scenario using a GPS along different Lissajous curves [45] in a two-dimensional space (depicted by the red trajectories in Fig. 2). The GPS readings are simulated at a frequency of 100 Hz over a duration of 10 seconds and are further corrupted by an additive noise following a Gaussian distribution $\mathcal{N}(\underline{0}_2, 0.01 \mathbf{I}_2)$.

We configure the TriS model with a state vector $\underline{x}_k \in \mathbb{R}^8$ that concatenates the recurrent control points $\{\underline{c}_{n_k-i}\}_{i=0}^3 \subset \mathbb{R}^2$ of temporal interval $\tau = 0.1$ second. To model the GPS sensing, we concretize the generic formulation of the measurement model in (9) to be

$$\underline{z}_k = \Lambda_{t_k^z} \underline{x}_k + \underline{v}_k, \quad \text{with} \quad \Lambda_{t_k^z} = (\Omega \underline{u}_{t_k^z})^\top \otimes \mathbf{I}_2 \quad (17)$$

being the coefficient matrix for position interpolation at $t_k^z \in (t_{n_{k-1}}, t_{n_k}]$. $\underline{u}_{t_k^z} = (t_k^z - t_{n_{k-1}})/\tau$ denotes the normalized time instant according to (2). The measurement noise is set to be zero-mean Gaussian-distributed with $\underline{v}_k \sim \mathcal{N}(\underline{0}_2, \mathbf{R}_k)$, where $\mathbf{R}_k = 0.01 \mathbf{I}_2$. Given the linear observation function in (17), the observation matrix for spline-embedded recursive estimation in Alg. 1 follows $\mathbf{H}_k = \Lambda_{t_k^z}$ according to (14). Furthermore, we exploit the expression of the process model in (13) for state propagation. The process noise is Gaussian-distributed following $\mathcal{N}(\underline{0}_8, \mathbf{Q})$, where the covariance

$$\mathbf{Q} = (0.02 \mathbf{I}_6) \oplus (0.1 \mathbf{I}_2),$$

with \oplus denoting the direct sum as introduced in Sec. II.

As shown by the blue curves in Fig. 2, the proposed method delivers accurate tracking results along different trajectories. In Fig. 3, we illustrate the estimated uncertainty along the sequence in Fig. 2-(D) via the probabilistic interpolation introduced in Sec. V-B in conjunction with downsampled measurements. These qualitative results are evident to show the efficacy of the proposed SERE scheme, including the continuous-time probabilistic interpretation of the motion estimates.

VI. EVALUATION

We now conduct an in-depth evaluation of the proposed SERE scheme using a multi-sensor setup for motion estimation. Comparisons with conventional recursive filtering scheme will be presented based on numerical results, followed by discussions on the configuration of the approach.

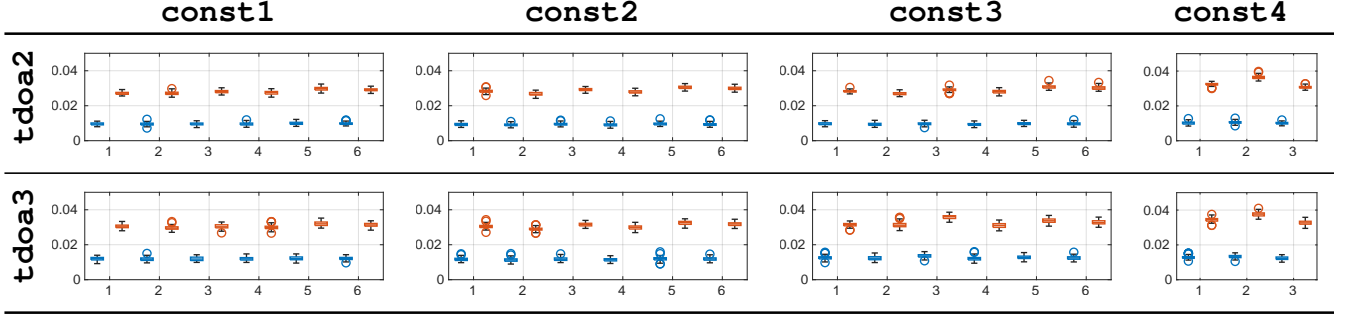


Fig. 4: Summary of the evaluation results on Syn-UTIL. Numbers on the horizontal axes denote `trial#` in `const1` to `const3` and `trial1-traj#` in `const4`. The vertical axes denote RMSEs w.r.t. ground truth, and their distributions on each sequence are plotted using the `boxchart` function of default setting in Matlab. The proposed spline-embedded recursive estimation scheme (blue) delivers consistently superior tracking accuracy over the baseline method (red).

A. Real-World-Based Synthetic Data Set

We create a synthesized scenario for motion estimation in sensor networks using time-of-arrival (ToA) and acceleration measurements. The UTIL data set is exploited as a real-world reference [46], where asynchronous UWB and IMU readings are recorded onboard a moving quadrotor platform. We choose a subset of UTIL that comprises all distinctive trajectories of autonomous maneuvers. This yields a total of 42 sequences under different UWB anchor constellations (`const1-4`) and operation modes (`tdoa2` and `tdoa3`). We adopt the ground truth trajectories to simulate the accelerometer (w.r.t. the world frame) and ToA data at the original time instants of the IMU (1000 Hz) and UWB (200 - 500 Hz) readings of UTIL, respectively. In addition, we corrupt these generated observations with additive zero-mean Gaussian noises of covariances $\mathbf{R}^a = 0.01 \mathbf{I}_3$ and $\mathbf{R}^u = 0.01$ for the accelerometer and ToA readings, respectively. In the subsequent evaluation, we refer to this synthetic data set as Syn-UTIL.

B. Setup

Given the previously synthesized evaluation scenario, we now establish the TriS model used in the SERE scheme. We configure the temporal interval of control points to be $\tau = 1$ second. At step k , the state vector comprising the recurrent control points $\{\mathbf{c}_{t_k-i}\}_{i=0}^3 \subset \mathbb{R}^3$ follows $\underline{\mathbf{x}}_k \in \mathbb{R}^{12}$. The process model in (13) is employed for state propagation, and the additive noise term $\underline{\mathbf{w}}_{k+1}$ therein follows a zero-mean Gaussian distribution $\mathcal{N}(\underline{0}_{12}, \mathbf{Q})$, with

$$\mathbf{Q} = (0.02 \times 10^{-5} \mathbf{I}_9) \oplus (10^{-2} \mathbf{I}_3).$$

The measurement models at time instant t_k^z are formulated according to (9) as

$$\begin{aligned} \mathbf{z}_k^a &= \ddot{\Lambda}_{t_k} \underline{\mathbf{x}}_k + \underline{\mathbf{v}}_k^a \quad \text{or} \\ \mathbf{z}_k^u &= \|\Lambda_{t_k} \underline{\mathbf{x}}_k - \underline{\mathbf{l}}_k\| + \mathbf{v}_k^u, \end{aligned} \quad (18)$$

given an accelerometer or a ToA measurement, respectively. Here, $\underline{\mathbf{l}}_k$ in the range observation denotes the position of the anchor indexed at t_k^z according to the original setting in UTIL. The noise terms $\underline{\mathbf{v}}_k^a$ and \mathbf{v}_k^u follow zero-mean Gaussian distributions of covariances \mathbf{R}^a and \mathbf{R}^u as described in Sec. VI-A, respectively. Given the expressions in (18), the observation matrices of the accelerometer and ToA measurement models can be derived according to (14) as

$$\begin{aligned} \mathbf{H}_k^a &= \ddot{\Lambda}_{t_k} \quad \text{and} \\ \mathbf{H}_k^u &= (\Lambda_{t_k} \underline{\mathbf{x}}_k - \underline{\mathbf{l}}_k)^\top \Lambda_{t_k} / \|\Lambda_{t_k} \underline{\mathbf{x}}_k - \underline{\mathbf{l}}_k\|, \end{aligned} \quad (19)$$

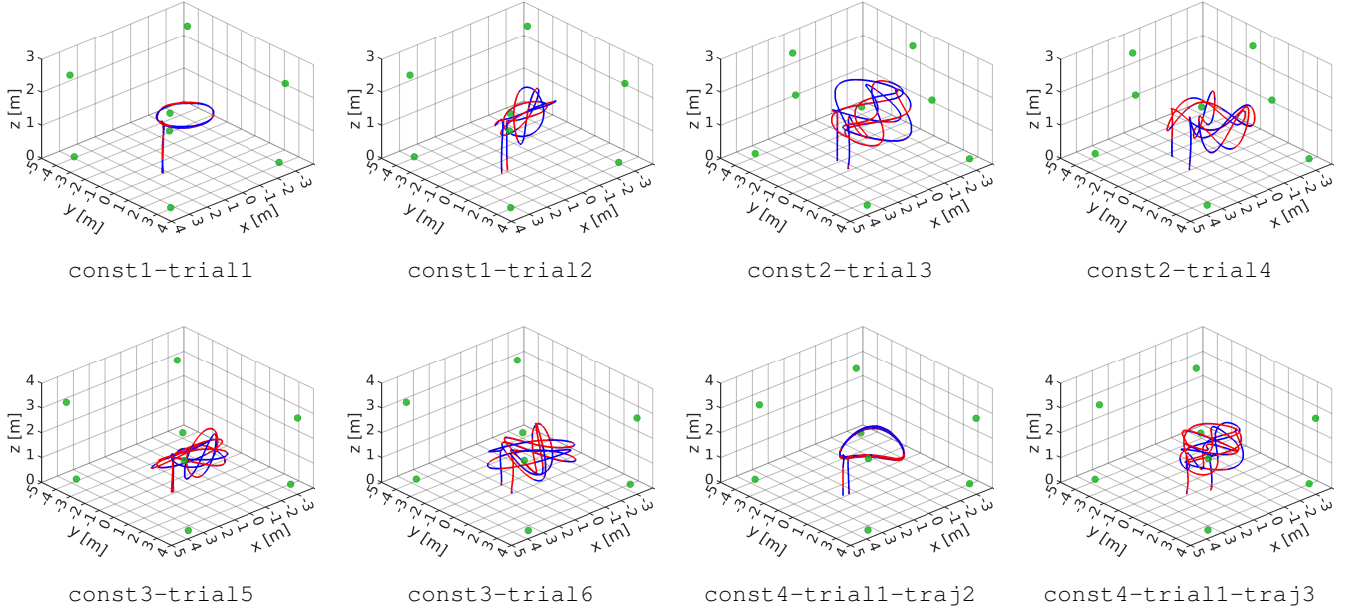


Fig. 5: Representative results given by the SERE scheme on sequences of Syn-UTIL-tdoa2 with all shapes of trajectories. Blue and red curves depict the estimates and corresponding ground truth, respectively, and green dots denotes coordinates of the anchors for ToA ranging.

respectively. We then perform the proposed spline-embedded recursive estimation on the recurrent control points according to Alg. 1, and the trajectory estimates are obtained online via the kinematic interpolation given in (6).

For comparison with the conventional recursive estimation scheme, we implement an EKF as the baseline. It estimates a state vector comprising the position and velocity. The prediction and update steps are scheduled asynchronously according to the multi-sensor fusion scenario. Given an accelerometer reading, a prediction step is conducted under the assumption of constant acceleration since the previous measurement. Upon the arrival of a ToA measurement, we first propagate the state via the constant-acceleration model using the previous accelerometer reading. Afterward, an EKF update step is performed to fuse the range measurement and deliver the posterior estimate.

C. Results

For evaluating the estimation schemes, we compute the root mean squared error (RMSE) of the position estimates w.r.t. the ground truth throughout the trajectory. Overall 100 Monte Carlo runs are performed on each of the 42 sequences in Syn-UTIL, and the resulting RMSE distributions are summarized in Fig. 4. Compared with the EKF of conventional design, the spline-embedded estimation scheme enables considerable improvement on tracking accuracy across all sequences of various settings. Furthermore, it only requires storage of the underlying control points occurring at a frequency of 1 Hz (given $\tau = 1s$) and delivers continuous motion trajectories over time, whereas the baseline method adopts discrete-time states at the rate of multi-modal measurements (asynchronous between 200 and 1000 Hz).

In Fig. 5, we select the sequences that encompass all different shapes of trajectories in Syn-UTIL to demonstrate representative tracking results given by SERE. The proposed method delivers inherently smooth trajectory estimates with close alignment to the ground truth. To further highlight the strength of spline embedding in noise adaptation, we perform additional tests on trial4 and trial6 of tdoa2 in Syn-UTIL under increased noise level of ToA ranging ($R^u = 0.1$). As shown in the plots of top view in Fig. 6, the proposed SERE scheme produces accurate trajectory estimates with inherent kinematic consistency thanks to the B-spline intermediate in the TriS model. In contrast, the baseline method exhibits

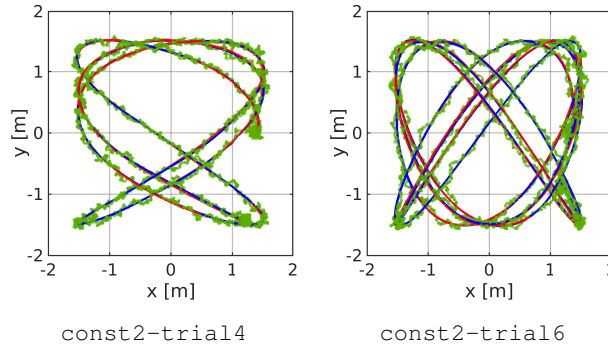


Fig. 6: Exemplary trajectory estimates given by the proposed (blue) and conventional (green) schemes w.r.t. ground truth (red). As introduced in Sec. VI-C, two sequences from `Syn-UTIL-tdoa2` are adopted under increased ToA measurement noise level for comparison.

clearly inferior tracking performance and delivers physically infeasible motion transitions due to the conventional state-space formulation.

D. Discussion

Achieving high performance in state estimation using spline embedding requires proper configurations of the system. In this regard, we provide insights on tuning two major parameters as follows.

1) *Temporal interval*: The interval τ for placing control points in the time domain is a global parameter for embedding B-splines in recursive estimation. In principle, a smaller value of τ allows for more detailed modeling of dynamical motions. However, this also requires higher rate of sensor measurements for more frequent state propagation and correspondingly more memory consumption for state storage.

2) *Process noise*: Tuning the process noise in deploying the SERE scheme follows common practice for conventional stochastic filtering. This typically refers to criteria regarding tracking accuracy, adaptation speed, noise sensitivity, etc [47]. According to (13), the last three recurrent control points of the previous state are preserved during system propagation, with a new control point to be added for spline extension. Therefore, we typically construct \mathbf{Q} with the following diagonal structure

$$\mathbf{Q} = (\omega \mathbf{I}_{3d}) \oplus (\nu \mathbf{I}_d), \quad (20)$$

where usually a higher uncertainty is assigned to the newly added control point compared to the preserved ones, namely, $\omega < \nu$. During the update step, the latest recurrent control point usually obtains a higher gain compared with the other ones. In general, a recurrent control point receives less gain over time until being removed from the state vector, and its estimate is then fixed.

To further justify our insights to parameter tuning provided previously, we now conduct a dedicated study using sequence `const1-trial2-tdoa2` in `Syn-UTIL` under the noise level of $\mathbf{R}^u = 0.1$ for the ToA data (The rest setup stays the same as introduced in Sec. VI-A). The configuration of process noise follows the general expression in (20), with $\omega \in \{0.1, 0.01, 0.001\}$ and $\nu = 0.1$ controlling the noise levels of preserving and adding recurrent control points, respectively. Meanwhile, the temporal interval of control points varies among $\tau \in \{0.1, 1, 6\}$.

Fig. 7 depicts the trajectory estimates given by SERE using the nine different parameter sets. When fixing the temporal interval τ , reducing the relative uncertainty of preserving and adding recurrent control points (smaller ω/ν) leads to better tracking accuracy. Given the same process noise, coarser control points in time domain (larger τ) induce less memory consumption for state storage, however, insufficiency in estimating complex trajectories. A small temporal interval τ can mitigate this issue, but it also results in overly dynamic motion estimates due to the fixed measurement rates. In practice, setting up the proposed SERE scheme often comes to trade-offs among multiple factors, including motion dynamics, sensor data rate and hardware constraints, etc.

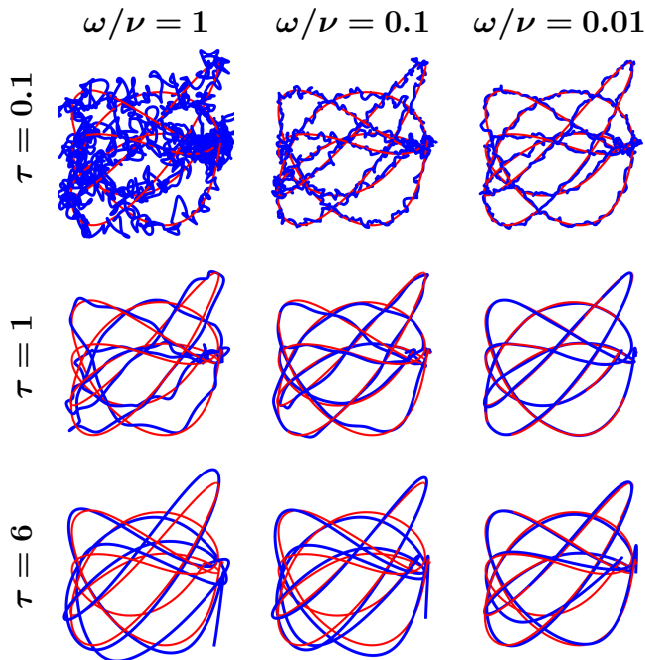


Fig. 7: Trajectory estimates (blue) given by SERE w.r.t. ground truth (red) on `const1-trial2-tdoa2` in top view. Various configurations of the temporal interval τ and noise ratios ω/ν for propagating recurrent control points are tested as discussed in Sec. VI-D. The parameter set $(\omega/\nu, \tau) = (0.01, 1)$ leads to the best tracking accuracy.

VII. CONCLUSION

In this work, we have conducted a principled study on a novel continuous-time framework for recursive state estimation. The so-called spline-state-space (TriS) model has been established by embedding B-splines in state-space modeling as a continuous-time intermediate, which decouples propagating discrete-time states of recurrent control points from incorporating asynchronous sensor readings. Based thereon, we have established the spline-embedded recursive estimation (SERE) scheme and have introduced corresponding technique for probabilistic modeling of dynamical motion estimates. The proposed estimation scheme has been validated in real-world-based synthesized scenario for continuous-time state estimation using a ToA-accelerometer setting. Compared with conventional recursive filtering, it demonstrates several advantages, including improved tracking accuracy, kinematic feasibility, storage consumption, and deployment flexibility.

There still exists much potential to exploit the SERE scheme. One promising direction for enhancing the current design is to develop dedicated methods for automatic system tuning. Another straightforward extension is to enable six-DoF motion estimation by incorporating spline modeling of spatial rotations [7], [48]. Moreover, B-splines atop control points of nonuniform temporal interval should be considered to improve the efficiency of state representation. Also, applying the proposed SERE scheme to extensive real-world applications of various multi-sensor settings is appealing [36], [37], [49]. This can, in turn, provides valuable insights for characterizing and improving the overall design of spline-based estimation schemes.

REFERENCES

- [1] X. Gao, J. Silv erio, E. Pignat, S. Calinon, M. Li, and X. Xiao, "Motion mappings for continuous bilateral teleoperation," *IEEE Robotics and Automation Letters*, vol. 6, no. 3, pp. 5048–5055, 2021.

- [2] L. An and G.-H. Yang, "State estimation under sparse sensor attacks: A constrained set partitioning approach," *IEEE Transactions on Automatic Control*, vol. 64, no. 9, pp. 3861–3868, 2019.
- [3] K. Ding, X. Ren, A. S. Leong, D. E. Quevedo, and L. Shi, "Remote state estimation in the presence of an active eavesdropper," *IEEE Transactions on Automatic Control*, vol. 66, no. 1, pp. 229–244, 2021.
- [4] S. Piperakis, D. Kanoulas, N. G. Tsagarakis, and P. Trahanias, "Outlier-robust state estimation for humanoid robots," in *Proceedings of the IEEE/RSJ International Conference on Intelligent Robots and Systems*, 2019, pp. 706–713.
- [5] J. Engel, J. Sturm, and D. Cremers, "Camera-based navigation of a low-cost quadcopter," in *Proceedings of the IEEE/RSJ International Conference on Intelligent Robots and Systems*, 2012, pp. 2815–2821.
- [6] K. Li, M. Li, and U. D. Hanebeck, "Towards high-performance solid-state-LiDAR-inertial odometry and mapping," *IEEE Robotics and Automation Letters*, vol. 6, no. 3, pp. 5167–5174, 2021.
- [7] K. Li, Z. Cao, and U. D. Hanebeck, "Continuous-time ultra-wideband-inertial fusion," *IEEE Robotics and Automation Letters*, vol. 8, no. 7, pp. 4338–4345, 2023.
- [8] H. Möls, K. Li, and U. D. Hanebeck, "Highly parallelizable plane extraction for organized point clouds using spherical convex hulls," in *Proceedings of the IEEE International Conference on Robotics and Automation*, 2020, pp. 7920–7926.
- [9] M. Bloesch, M. Burri, S. Omari, M. Hutter, and R. Siegwart, "Iterated extended Kalman filter based visual-inertial odometry using direct photometric feedback," *The International Journal of Robotics Research*, vol. 36, no. 10, pp. 1053–1072, 2017.
- [10] F. Gustafsson, F. Gunnarsson, N. Bergman, U. Forssell, J. Jansson, R. Karlsson, and P.-J. Nordlund, "Particle filters for positioning, navigation, and tracking," *IEEE Transactions on Signal Processing*, vol. 50, no. 2, pp. 425–437, 2002.
- [11] S. M. Kay, *Fundamentals of statistical signal processing: Estimation theory*. Prentice-Hall, Inc., 1993.
- [12] H. Li, D. Medina, J. Vilà-Valls, and P. Closas, "Robust variational-based Kalman filter for outlier rejection with correlated measurements," *IEEE Transactions on Signal Processing*, vol. 69, pp. 357–369, 2021.
- [13] N. Bono Rossello, R. F. Carpio, A. Gasparri, and E. Garone, "Information-driven path planning for UAV with limited autonomy in large-scale field monitoring," *IEEE Transactions on Automation Science and Engineering*, vol. 19, no. 3, pp. 2450–2460, 2022.
- [14] S. P. Talebi and S. Werner, "Distributed Kalman filtering and control through embedded average consensus information fusion," *IEEE Transactions on Automatic Control*, vol. 64, no. 10, pp. 4396–4403, 2019.
- [15] S. Bultmann, K. Li, and U. D. Hanebeck, "Stereo visual SLAM based on unscented dual quaternion filtering," in *Proceedings of the International Conference on Information Fusion*, 2019, pp. 1–8.
- [16] J. Sola, "Quaternion kinematics for the error-state Kalman filter," *arXiv preprint arXiv:1711.02508*, 2017.
- [17] K. Li, F. Pfaff, and U. D. Hanebeck, "Unscented dual quaternion particle filter for SE(3) estimation," *IEEE Control Systems Letters*, vol. 5, no. 2, pp. 647–652, 2021.
- [18] K. Li, "On-manifold recursive Bayesian estimation for directional domains," Ph.D. dissertation, Karlsruhe Institute of Technology, 2022.
- [19] G. Grisetti, R. Kümmerle, C. Stachniss, and W. Burgard, "A tutorial on graph-based SLAM," *IEEE Intelligent Transportation Systems Magazine*, vol. 2, no. 4, pp. 31–43, 2010.
- [20] H. Strasdat, J. M. M. Montiel, and A. J. Davison, "Real-time monocular SLAM: Why filter?" in *Proceedings of the IEEE International Conference on Robotics and Automation*, 2010, pp. 2657–2664.
- [21] S. Leutenegger, S. Lynen, M. Bosse, R. Siegwart, and P. Furgale, "Keyframe-based visual-inertial odometry using nonlinear optimization," *The International Journal of Robotics Research*, vol. 34, no. 3, pp. 314–334, 2015.
- [22] A. Reinke, M. Palieri, B. Morrell, Y. Chang, K. Ebadi, L. Carlone, and A.-A. Agha-Mohammadi, "LOCUS 2.0: Robust and computationally efficient LiDAR odometry for real-time 3D mapping," *IEEE Robotics and Automation Letters*, vol. 7, no. 4, pp. 9043–9050, 2022.
- [23] T. Qin, P. Li, and S. Shen, "VINS-Mono: A robust and versatile monocular visual-inertial state estimator," *IEEE Transactions on Robotics*, vol. 34, no. 4, pp. 1004–1020, 2018.
- [24] S. Cao, X. Lu, and S. Shen, "GVINS: Tightly coupled GNSS–visual–inertial fusion for smooth and consistent state estimation," *IEEE Transactions on Robotics*, vol. 38, no. 4, pp. 2004–2021, 2022.
- [25] D. Wisth, M. Camurri, and M. Fallon, "VILENS: Visual, inertial, LiDAR, and leg odometry for all-terrain legged robots," *IEEE Transactions on Robotics*, vol. 39, no. 1, pp. 309–326, 2023.
- [26] S. Särkkä, *Bayesian filtering and smoothing*. Cambridge university press, 2013, no. 3.
- [27] P. Axelsson and F. Gustafsson, "Discrete-time solutions to the continuous-time differential Lyapunov equation with applications to Kalman filtering," *IEEE Transactions on Automatic Control*, vol. 60, no. 3, pp. 632–643, 2015.
- [28] S. Anderson and T. D. Barfoot, "Towards relative continuous-time SLAM," in *Proceedings of the IEEE International Conference on Robotics and Automation*, 2013, pp. 1033 – 1040.
- [29] E. Mueggler, G. Gallego, and D. Gallego, "Continuous-time trajectory estimation for event-based vision sensors," in *Robotics: Science and Systems*, 2015.
- [30] G. Cioffi, T. Cieslewski, and D. Scaramuzza, "Continuous-time vs. discrete-time vision-based SLAM: A comparative study," *IEEE Robotics and Automation Letters*, vol. 7, no. 2, pp. 2399–2406, 2022.
- [31] K. Qin, "General matrix representations for B-splines," in *Proceedings Pacific Graphics' 98. Sixth Pacific Conference on Computer Graphics and Applications (Cat. No. 98EX208)*, 1998, pp. 37–43.
- [32] P. Furgale, T. D. Barfoot, and G. Sibley, "Continuous-time batch estimation using temporal basis functions," in *Proceedings of the IEEE International Conference on Robotics and Automation*, 2012, pp. 2088–2095.
- [33] H. Sommer, J. R. Forbes, R. Siegwart, and P. Furgale, "Continuous-time estimation of attitude using B-splines on Lie groups," *Journal of Guidance, Control, and Dynamics*, vol. 39, no. 2, pp. 242–261, 2016.
- [34] E. Mueggler, G. Gallego, H. Rebecq, and D. Scaramuzza, "Continuous-time visual-inertial odometry for event cameras," *IEEE Transactions on Robotics*, vol. 34, no. 6, pp. 1425–1440, 2018.

- [35] D. Hug, P. Bänniger, I. Alzugaray, and M. Chli, “Continuous-time stereo-inertial odometry,” *IEEE Robotics and Automation Letters*, vol. 7, no. 3, pp. 6455–6462, 2022.
- [36] Y. Z. Ng, B. Choi, R. Tan, and L. Heng, “Continuous-time radar-inertial odometry for automotive radars,” in *Proceedings of the IEEE/RSJ International Conference on Intelligent Robots and Systems*, 2021, pp. 323–330.
- [37] J. Lv, K. Hu, J. Xu, Y. Liu, X. Ma, and X. Zuo, “CLINS: Continuous-time trajectory estimation for LiDAR-inertial system,” in *IEEE/RSJ International Conference on Intelligent Robots and Systems*, 2021, pp. 6657–6663.
- [38] A. J. Yang, C. Cui, I. A. Bârsan, R. Urtasun, and S. Wang, “Asynchronous multi-view SLAM,” in *Proceedings of the IEEE International Conference on Robotics and Automation*, 2021, pp. 5669–5676.
- [39] C. Sommer, V. Usenko, D. Schubert, N. Demmel, and D. Cremers, “Efficient derivative computation for cumulative B-splines on Lie groups,” in *Proceedings of the IEEE/CVF Conference on Computer Vision and Pattern Recognition*, 2020, pp. 11 148–11 156.
- [40] M. Persson, G. Häger, H. Ovrén, and P.-E. Forssén, “Practical pose trajectory splines with explicit regularization,” in *Proceedings of the International Conference on 3D Vision*, 2021, pp. 156–165.
- [41] M. Harashima, L. Ferrari, and P. Sankar, “Spline approximation using Kalman filter state estimation,” *IEEE Transactions on Circuits and Systems II: Analog and Digital Signal Processing*, vol. 44, no. 5, pp. 421–424, 1997.
- [42] J. Jauch, F. Bleimund, S. Rhode, and F. Gauterin, “Recursive B-spline approximation using the Kalman filter,” *Engineering Science and Technology, an International Journal*, vol. 20, no. 1, pp. 28–34, 2017.
- [43] K. H. Rosen, *Handbook of discrete and combinatorial mathematics*. CRC press, 1999.
- [44] H. D. Macedo and J. N. Oliveira, “Typing linear algebra: A biproduct-oriented approach,” *Science of Computer Programming*, vol. 78, no. 11, pp. 2160–2191, 2013.
- [45] K. Gamagedara, T. Lee, and M. Snyder, “Quadrotor state estimation with IMU and delayed real-time kinematic GPS,” *IEEE Transactions on Aerospace and Electronic Systems*, vol. 57, no. 5, pp. 2661–2673, 2021.
- [46] W. Zhao, A. Goudar, X. Qiao, and A. P. Schoellig, “UTIL: An ultra-wideband time-difference-of-arrival indoor localization dataset,” *arXiv preprint arXiv:2203.14471*, 2022.
- [47] F. Gustafsson and F. Gustafsson, *Adaptive filtering and change detection*. Wiley New York, 2000, vol. 1.
- [48] K. Li, F. Pfaff, and U. D. Hanebeck, “Grid-based quaternion filter for SO(3) Estimation,” in *Proceedings of the European Control Conference*, 2020, pp. 1738–1744.
- [49] K. Li, G. Kurz, L. Bernreiter, and U. D. Hanebeck, “Simultaneous localization and mapping using a novel dual quaternion particle filter,” in *Proceedings of the International Conference on Information Fusion*, 2018, pp. 1668–1675.